Adaptive Distance Protection Based on Analytical Model of Additional Impedance for Inverter-Interfaced Renewable Power Plant During Asymmetrical Faults

Chenxu Chao, Xiaodong Zheng, *Senior Member*, *IEEE*, Yang Weng, *Senior Member*, Yu Liu, *Member*, *IEEE*, Piao Gao, Nengling Tai, *Member*, *IEEE*

***Abstract*—Due to the limited amplitude and controlled phase of current supplied by inverter-interfaced renewable power plant (IIRPP), the distance protection on IIRPP-side of the outgoing line of IIRPP fails to accurately reflect the fault distance, so it may malfunction. The composite sequence network of the outgoing line of IIRPP with the control objective of eliminating the negative-sequence current during asymmetrical faults is analyzed, and an adaptive distance protection based on analytical model of additional impedance is proposed in this study. Based on the open circuit property of IIRPP-side in negative-sequence network, the equivalent impedance of power grid and the current at the fault point are calculated in real-time by local measurements, which are substituted into the analytical model of additional impedance to recognize the fault location. The proposed protection solves the poor tolerance problem to fault resistance of distance protection in the system with weak sources. In addition, the proposed protection can adapt to the change of operation mode of power grid and the requirements of reactive power support of IIRPP in grid codes (GCs) of different regions. PSCAD/EMTDC test results verify the effectiveness of proposed protection.**

***Index Terms*—Inverter-interfaced renewable power plant, distance protection, fault resistance, asymmetrical faults, outgoing line**

I. Introduction

With the increasingly prominent environmental problems and the development of power electronics technology, inverter-interfaced renewable energy power generation is increasingly applied [1]. Distance protection is widely used as main protection and backup protection in transmission lines [2],[3]. However, due to the influence of inverter control, the current supplied by inverter-interfaced renewable power plant (IIRPP) presents the characteristics of the limited amplitude and controlled phase, which is different from that of current supplied by synchronous generator (SG). As a result, the distance protection on IIRPP-side may malfunction during non-metallic faults[2].

In the systems with SG, the methods to improve the ability of tolerance to fault resistance of distance protection mainly include adaptive distance protection based on boundary adjustment, impedance complex plane and voltage phasor plane [4]-[10]. By adjusting trip boundaries, the adaptive distance protection based on boundary adjustment can operate reliably during non-metallic faults [4],[5]. Due to the weak infeed of IIRPP, the trip boundary is too large, causing the overreach of distance protection. In addition, this kind of protection needs to obtain the equivalent impedance of power grid, which requires communication. The principle of distance protection based on impedance complex plane is to calculate the phase of additional impedance by local negative-sequence current, and then calculate the actual fault location[6],[7],[8]. The principle of distance protection based on voltage phasor plane is to get the voltage characteristics during internal and external faults by analyzing the voltage phasor plane [9],[10]. The IIRPP with the control objective of eliminating the negative-sequence current does not output the negative-sequence current [11], and the power-frequency sequence impedance of IIRPP is not constant [12]. Therefore, there are large errors when these two methods are applied to the outgoing line of IIRPP. The traditional methods to improve the ability of tolerance to fault resistance of distance protection is invalid in outgoing line of IIRPP.

To cope with the poor tolerance problem to fault resistance of distance protection in the system with weak sources, some scholars put forward improved distance protection schemes [13]-[16]. In [13], a new expression of measured impedance containing zero-sequence current was proposed. The ability of tolerance to fault resistance of distance protection during phase to phase to ground (PPG) faults is improved, and a pilot protection scheme is proposed to remove phase to phase (PP) faults. Reference [14] and [15] proposed the protection schemes based on time delay, which eliminates the influence of fault

This work was partially supported by National Natural Science Foundation of China (51877135), Shanghai Rising-Star Program (18QA1402100) and National Key Research and Development Program of China (2016YFB0900600).

C. Chao, X. Zheng (Corresponding author), N. Tai and P. Gao are with Key Laboratory of Control of Power Transmission and Conversion (Ministry of Education), Shanghai Jiao Tong University, Shanghai 200240, China, Shanghai, 200240, China. (Corresponding author mail: xiaodongzheng@sjtu.edu.cn).

Y. Weng is with the School of Electrical, Computer and Energy Engineering, Arizona State University, Tempe, AZ 85282 USA (e-mail: yang.weng@asu.edu).

Y. Liu is with the School of Information Science and Technology, Shanghai Tech University, Shanghai, China, 201210 (email: liuyu.shanghaitech@gmail.com)

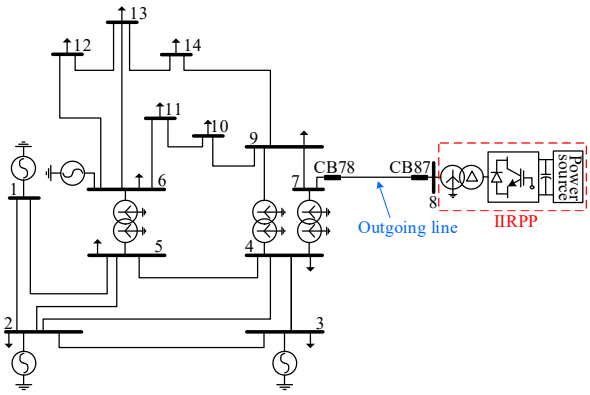

Fig. 1. Modified 138kV, 50Hz IEEE 14-bus system with IIRPP.

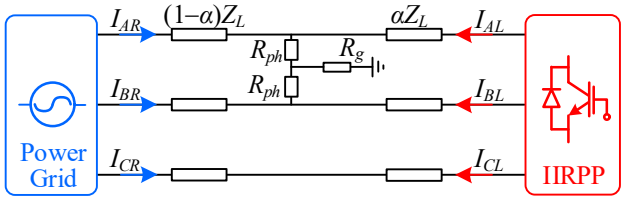

Fig. 2. Circuit diagram during PPG faults.

resistance on distance protection by giving priority to distance protection on grid-side. This kind of scheme has a long trip time. A distance protection based on inverter control was proposed in [16]. The phase of the additional impedance is adjusted to 0° by inverter control, which improves the reliability of quadrilateral impedance relay. In [17], a comprehensive dual current control scheme based protective relay was proposed. By improving the inverter control, the inverter can imitate the phase angles of a SG's fault current, which ensures the correct action of directional, phase-selection, and distance elements of a relay. However, it is necessary to adjust power factor (PF) during faults to meet the operation requirements of distance protection, which makes IIRPP fail to comply with local grid code (GC). The existing distance protection for the outgoing line of IIRPP has some disadvantages, such as requirements for communication, poor speediness, and failure to comply with GCs.

In order to solve the poor tolerance problem to fault resistance of distance protection in the system with weak sources, the composite sequence network of the outgoing line of IIRPP with the control objective of eliminating the negative-sequence current during asymmetrical faults is analyzed in detail, and an adaptive distance protection based on the analytical model of additional impedance is proposed. In proposed protection, the phase of additional impedance is calculated by local negative-sequence voltage, and the actual fault impedance can be obtained by the analytical model of additional impedance, which is employed to recognize the fault location. As a result, the proposed protection has strong tolerance to fault resistance and requires no communication. In addition, the proposed protection is adaptive to the change of operation mode of power grid, GCs, and the capacity of IIRPP. Finally, the effectiveness of proposed protection is verified in IEEE 14-bus system with IIRPP.

II. Problem Statement

A. Test System

Fig. 1 displays the modified 138kV, 50Hz IEEE 14-bus system with IIRPP. The point of common coupling (PCC) is Bus 8 and the rated power of IIRPP is 100MW. The length of outgoing line L87 is 40km. The impedance information of L87 is as follows: $Z_L^{(+)}=Z_L^{(-)}=0.0178+j0.314\Omega/km$ and $Z_L^{(0)}=0.158+j1.58\Omega/km$.

B. Operation Performance Analysis of Distance Protection

Due to the weak infeed and controlled current phase of IIRPP, the ability of tolerance to fault resistance of distance protection on the IIRPP-side of the outgoing line is poor. The specific analysis is as follows.

When a PP fault occurs in L87, the impedance measured by the phase A to phase B (AB) element of CB87 is as follows:

$$Z_{AB}=\alpha Z_L+\underbrace{R_{ph}\frac{I_{AR}+I_{AL}}{I_{AL}-I_{BL}}}_{Z_{add}} \tag{1}$$

where α is the fault location, Z_L is the positive-sequence impedance of L87, R_{ph} is the PP fault resistance, Z_{add} is the additional impedance caused by fault resistance, subscripts A, B, R, L represent phase A, phase B, the remote and the local measurements, respectively. Because of the weak infeed of IIRPP, the amplitude of denominator of Z_{add} is much smaller than that of numerator of Z_{add}, which makes the amplitude of Z_{add} large. In addition, the phase of Z_{add} may not be near 0° under GCs of different regions [2]. Therefore, the distance protection would malfunction during PP faults.

When a PPG fault occurs in L87, the circuit diagram is shown in Fig. 2, where R_g is the grounding fault resistance. The impedance measured by the phase A to ground (AG) and AB elements of CB87 is as follows:

$$Z_{AG}=\alpha Z_L+\underbrace{R_{ph}\frac{I_{AL}+I_{AR}}{I_{AL}+K^{(0)}I_L^{(0)}}+R_g\frac{I_{AL}+I_{AR}+I_{BL}+I_{BR}}{I_{AL}+K^{(0)}I_L^{(0)}}}_{Z_{add}} \tag{2}$$

$$Z_{AB}=\alpha Z_L+\underbrace{R_{ph}\left(1+\frac{I_{AR}-I_{BR}}{I_{AL}-I_{BL}}\right)}_{Z_{add}} \tag{3}$$

where $K^{(0)}$ is the zero-sequence compensation coefficient, and the superscript (0) represents the zero-sequence component. Similar to PP faults, the amplitude and phase characteristics of Z_{add} lead to the malfunction of the distance protection during PPG faults.

When a single phase to ground (SPG) fault occurs in L87, the impedance measured by the AG element of CB87 is as follows.

$$Z_{AG}=\alpha Z_L+R_g\frac{I_{AR}+I_{AL}}{I_{AL}+K^{(0)}I_L^{(0)}} \tag{4}$$

The amplitude of Z_{add} is mainly determined by the fault resistance and zero-sequence current, and the phase of Z_{add} is near 0° [2]. In most cases, the distance protection can operate normally during SPG faults, but overreach or underreach may occur when the fault occurs at the trip boundary.

In general, due to the weak infeed and controlled current

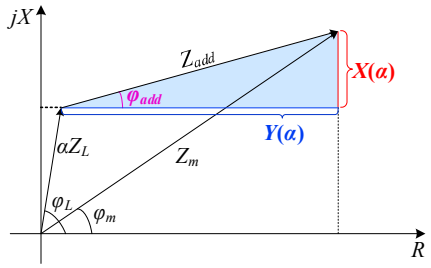

Fig. 3 Impedance complex plane during faults

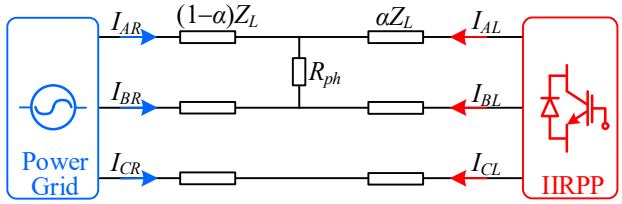

Fig. 4. Circuit diagram during PP faults.

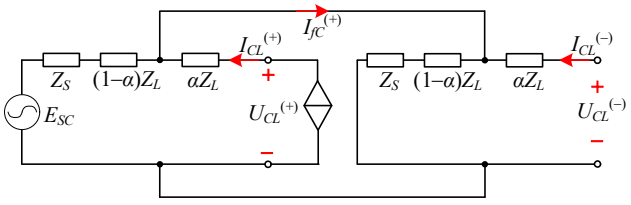

Fig. 5 Composite sequence network during PP faults

phase of IIRPP, the distance protection on IIRPP-side of the outgoing line may malfunction.

III. Principle of Proposed Protection

A. Analytical Model of Additional Impedance

During faults, the relationship between the actual fault impedance αZ_L, the additional impedance Z_{add} and the measured impedance Z_m is shown in Fig. 3. Where, φ_m is the phase of Z_m, φ_L is the phase of Z_L, and φ_{add} is the phase of Z_{add}. The analytical model of additional impedance is obtained from Fig. 3, as shown in the following equation:

$$X(\alpha)/Y(\alpha)=\tan(\varphi_{add}) \tag{5}$$

where $X(\alpha)=|Z_m|\sin\varphi_m-\alpha|Z_L|\sin\varphi_L$, $Y(\alpha)=|Z_m|\cos\varphi_m-\alpha|Z_L|\cos\varphi_L$, and $|\cdot|$ is the modulus of phasor.

B. Calculation of Fault Location During PP Faults

1) *Solution of Analytical Model of Additional Impedance*

The circuit diagram during a PP fault is shown in Fig. 4. The Z_m of AB element in CB87 is shown in the following equation:

$$Z_{AB}=\frac{U_{AL}-U_{BL}}{I_{AL}-I_{BL}}=\alpha Z_L+\underbrace{R_{ph}\frac{I_{fC}^{(+)}\angle-120°+I_{fC}^{(-)}\angle120°}{I_{AL}-I_{BL}}}_{Z_{add}} \tag{6}$$

where the subscript f represents the fault point, the superscript (+) and (–) represent the positive-sequence component and negative-sequence component, respectively. The composite sequence network of phase C is shown in Fig. 5. In Fig. 5, Z_S is the equivalent impedance of power grid; E_{SC} is the equivalent voltage source of phase C of power grid. Due to the control objective of negative-sequence current suppression, the negative-sequence current of IIRPP-side is negligible [18],[19]. Therefore, the IIRPP-side of the negative-sequence network is open circuit, and the following equation can be obtained.

$$I_{fC}^{(+)}=-I_{fC}^{(-)}=\frac{U_{CL}^{(-)}}{Z_S+(1-\alpha)Z_L} \tag{7}$$

Substituting (7) into Z_{add}, φ_{add} can be obtained, as shown in the following equation:

$$\varphi_{add}=\angle\frac{U_{CL}^{(-)}}{\left[Z_S+(1-\alpha)Z_L\right]\cdot I_{CL}^{(+)}} \tag{8}$$

where $\angle$ represents the phase of phasor. Substituting (8), $X(\alpha)$ and $Y(\alpha)$ into the analytical model of additional impedance (5), we obtain

$$\frac{|Z_m|\sin\varphi_m-\alpha|Z_L|\sin\varphi_L}{|Z_m|\cos\varphi_m-\alpha|Z_L|\cos\varphi_L}=\tan\left(\angle\frac{U_{CL}^{(-)}}{\left[Z_S+(1-\alpha)Z_L\right]\cdot I_{CL}^{(+)}}\right) \tag{9}$$

The solution of the equation (9) is shown in the following equation:

$$\alpha=\frac{-b\pm\sqrt{b^2-4ac}}{2a} \tag{10}$$

where a, b and c are expressed as follows.

$$\begin{cases} a=|Z_L|^2\cdot\sin(2\varphi_L-M) \\ b=|Z_L|\cdot|Z_m|\cdot\sin(M-\varphi_m-\varphi_L) \\ \quad +|Z_L|\cdot|Z_S|\cdot\sin(M-\varphi_S-\varphi_L) \\ \quad +|Z_L|^2\cdot\sin(M-2\varphi_L) \\ c=|Z_S|\cdot|Z_m|\cdot\sin(\varphi_S+\varphi_m-M) \\ \quad +|Z_L|\cdot|Z_m|\cdot\sin(\varphi_L+\varphi_m-M) \\ M=\angle\left(U_{CL}^{(-)}/I_{CL}^{(+)}\right) \end{cases} \tag{11}$$

Equation (10) shows that α has two solutions. It is proved that the effective solution meets the following constraints, and the specific proof is shown in Appendix A:

$$\begin{cases} X(\alpha)/|X(\alpha)|=\sin h(\alpha)/|\sin h(\alpha)| \\ \alpha>0 \end{cases} \tag{12}$$

where $h(\alpha)$ is as follows.

$$h(\alpha)=\angle\frac{U_{CL}^{(-)}}{I_{CL}^{(+)}}-\arctan\frac{|Z_S|\sin\varphi_S+(1-\alpha)|Z_L|\sin\varphi_L}{|Z_S|\cos\varphi_S+(1-\alpha)|Z_L|\cos\varphi_L} \tag{13}$$

2) *Calculation of System Impedance*

The circuit diagram during normal operation and PP faults are shown in Fig. 6. According to Kirchhoff Voltage Law (KVL), there is the following equation during normal operation and PP faults:

$$\begin{cases} \left(U_{CL}^{[0]}-E_{SC}\right)/(Z_S+Z_L)=I_{CL}^{[0]} \\ \left(U_{CL}-E_{SC}\right)/(Z_S+Z_L)=I_{CL} \end{cases} \tag{14}$$

where the superscript [0] represents the measurement during normal operation. By solving the quadratic equation (14), Z_S

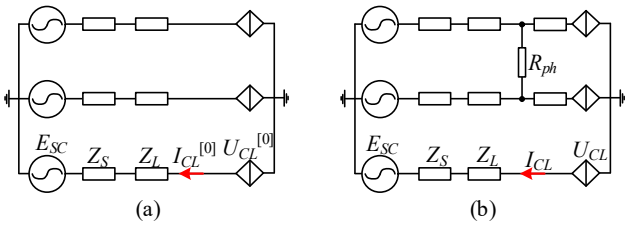

Fig. 6 Circuit diagram of outgoing line. (a) During normal operation. (b) During PP faults

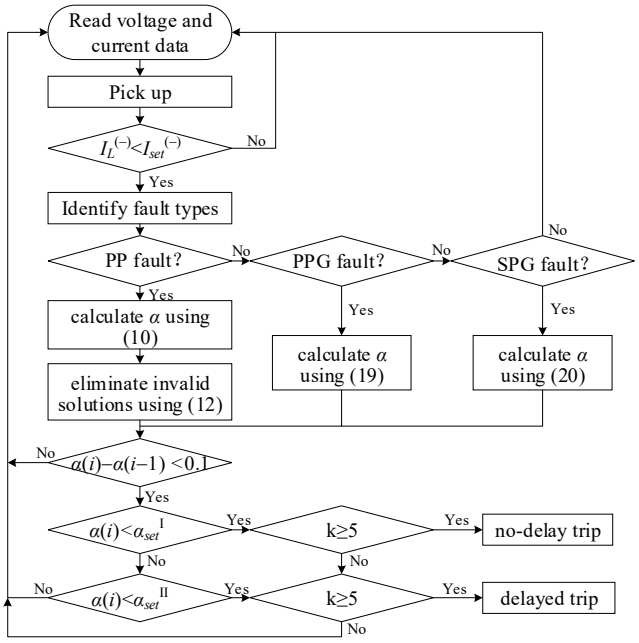

Fig. 7 Protection scheme

can be obtained as follows.

$$Z_S = \frac{U_{CL}^{[0]} - U_{CL} - \left(I_{CL}^{[0]} - I_{CL}\right)\cdot Z_L}{I_{CL}^{[0]} - I_{CL}} \tag{15}$$

It can be seen from (15) that Z_S can be calculated by local measurements. Therefore, the fault location can be obtained by local measurements.

C. Calculation of Fault Location During PPG and SPG Faults

In [13], a new formula of Z_m is devised to prevent maloperation of distance protection during PPG faults. The new expression of Z_m in [13] and its transformation are shown in the following equation.

$$\begin{aligned} Z_m^{new} &= \frac{U_{AL}+U_{BL}}{I_{AL}+I_{BL}+2K^{(0)}I_L^{(0)}} \\ &= \alpha Z_L + \underbrace{\left(R_{ph}+2R_g\right)\frac{3I_f^{(0)}}{I_{AL}+I_{BL}+2K^{(0)}I_L^{(0)}}}_{Z_{add}} \end{aligned} \tag{16}$$

The relationship between $I_L^{(0)}$ and $I_f^{(0)}$ can be obtained from [6], as shown in the following equation:

$$I_L^{(0)} = C^{(0)}\cdot I_f^{(0)} \tag{17}$$

where $C^{(0)}$ is the branching coefficient of zero-sequence current on IIRPP-side. Since $C^{(0)}$ in the high-voltage system can be regarded as a constant[6],[20], φ_{add} can be obtained from the following equation.

$$\varphi_{add} = \angle\frac{I_L^{(0)}}{I_{AL}+I_{BL}+2K^{(0)}I_L^{(0)}} \tag{18}$$

Substituting (18) into the analytical model of additional impedance (5), the fault location during PPG faults can be obtained as shown in the following equation:

$$\alpha = \frac{\tan\left(\varphi_{add}\right)\cos\left(\varphi_m^{new}\right)+\sin\left(\varphi_m^{new}\right)}{\sin\left(\varphi_m^{new}\right)+\cos\left(\varphi_L\right)\tan\left(\varphi_{add}\right)\left|Z_L\right|/\left|Z_m^{new}\right|} \tag{19}$$

where φ_m^{new} is the phase of Z_m^{new}. The φ_{add} during SPG faults has been studied in detail in [6]. By substituting φ_{add} into (5), the fault location during SPG faults can be obtained as follows.

$$\alpha = \frac{\tan\left(\varphi_{add}\right)\cos\left(\varphi_m\right)+\sin\left(\varphi_m\right)}{\sin\left(\varphi_m\right)+\cos\left(\varphi_L\right)\tan\left(\varphi_{add}\right)\left|Z_L\right|/\left|Z_m\right|} \tag{20}$$

IV. Protection Scheme

If $I_L^{(-)}$, the negative-sequence current flowing through CB87, is greater than $I_{set}^{(-)}$, the setting value of negative-sequence current, during faults, the protection will return because the fault is a reverse fault. The $I_{set}^{(-)}$ can be adjusted according to the maximum negative-sequence current supplied by IIRPP. If the fault is a forward fault, the corresponding equation is selected according to the fault type to calculate α. Refer to [11] and [21] for the fault selection and phase selection technology in the systems with IIRPP.

The protection criteria are as follows:

1) The difference between α at the current sampling point and α at the previous sampling point is less than 0.1pu/ms.

2) α is less than the setting value (in this paper, the setting value of zone 1 is taken as 0.8, and that of zone 2 is taken as 1.2).

3) Five consecutive sampling points meet criteria 1) and 2).

Fig. 7 shows the protection flow chart, in which k represents the number of sampling points continuously meeting the criterion 1) and criterion 2).

V. Simulation Verification

Based on PSCAD/EMTDC, the simulation model of test system shown in Fig. 1 is built.

IIRPP has the ability of reactive power support during faults [22]. However, the requirements of GCs in different regions are different. The GCs of most European countries require IIRPPs to provide reactive power support during faults[2]; There is no requirement for IIRPPs to inject reactive current during faults in North American GC [2]; Chinese GC requires that IIRPPs connected to the grid through lines of 500kV or above provide reactive power support during faults, while there is no requirement for IIRPPs connected to the grid through lines below 500 kV to provide reactive power support during faults [23]. To sum up, the reactive power support strategy of different GCs during faults can be summarized into two types: 1) no reactive power support and 2) providing reactive power support,

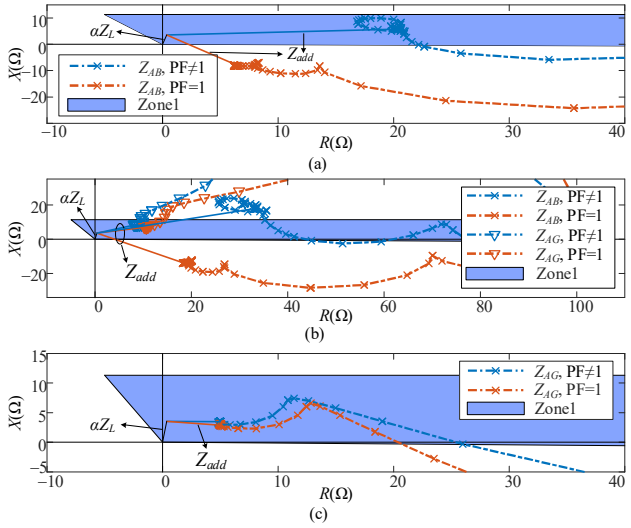

Fig. 8 The trace diagram of Z_m during faults at 50% of L87 with 10Ω fault resistance. (a) PP faults. (b) PPG faults. (c) SPG faults.

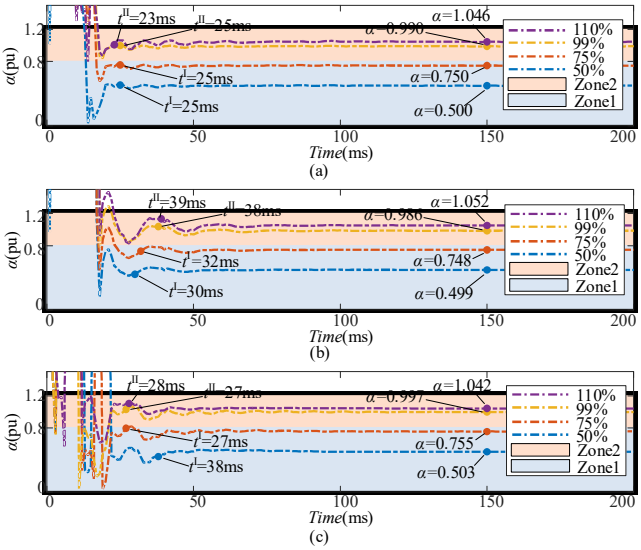

Fig. 9 Operation performance of proposed protection during PP faults. (a) R_{ph}=1Ω.(b) R_{ph}=10Ω.(c) R_{ph}=100Ω.

which are represented by PF=1 and PF≠1, respectively.

A. Operation Performance of Traditional Distance Protection

When asymmetric faults with 10Ω fault resistance occur at 50% of L87, Z_m of the AB and AG elements in CB87 is shown in Fig. 8. It can be seen from Fig. 8 that during PP and PPG faults, the AB elements fail to trip correctly in different GCs. Due to the existence of zero-sequence current, the AG elements operate correctly during PPG and SPG faults. However, the AG element fail to locate the fault accurately. Thus, the traditional distance protection may malfunction.

B. Operation Performance of Proposed Protection During PP Faults

If the IIRPP provides no reactive power support during faults, that is, PF=1, when a PP fault occurs at 50%, 75%, 99% and 110% of L87 with different fault resistance, the operation performance of proposed protection is shown in Fig. 9, in which

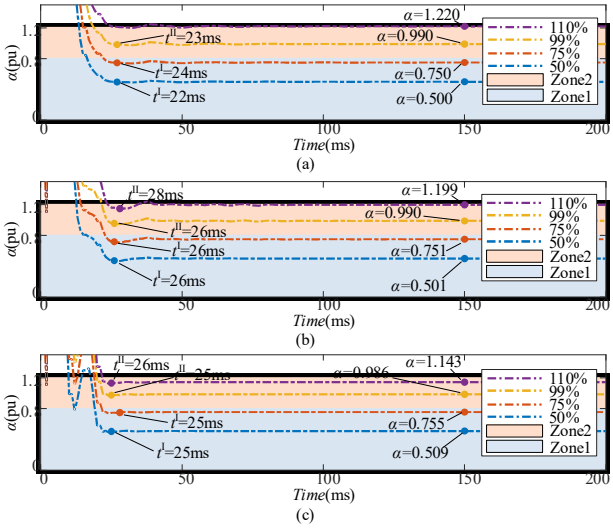

Fig. 10 Operation performance of proposed protection during PPG faults. (a)R_{ph}=R_g=1Ω. (b)R_{ph}=R_g=10Ω. (c)R_{ph}=R_g=100Ω.

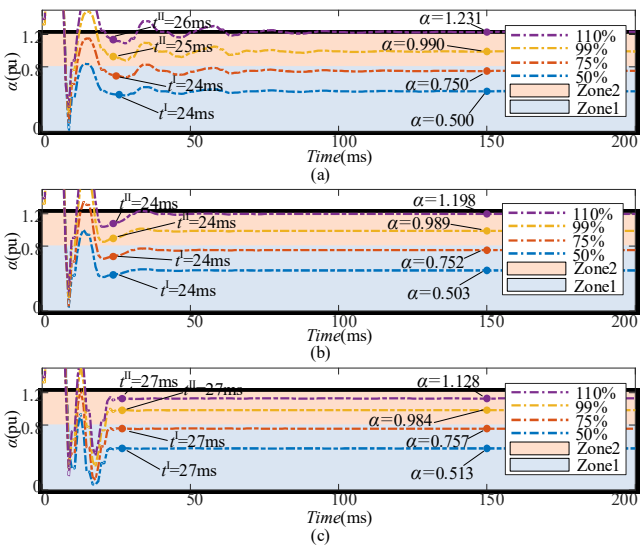

Fig. 11 Operation performance of proposed protection during SPG faults. (a)R_g=1Ω. (b)R_g=10Ω. (c)R_g=100Ω.

110% of L87 is located at L79.

In Fig. 9, t^{I} is the trip time of zone 1 and t^{II} is the trip time of zone 2. The proposed protection can accurately locate the fault during PP faults at L87. Therefore, the proposed protection can reliably clear PP faults at L87 and provide remote backup protection for L79. The trip signal can be sent out within 40ms after PP faults occurring. In conclusion, the proposed protection can operate correctly during PP faults and has strong tolerance to fault resistance.

C. Operation Performance of Proposed Protection During PPG and SPG Faults

When PPG and SPG faults occur at 50%, 75%, 99% and 110% of L87 with different fault resistance, the operation performance of proposed protection is shown in Fig. 10 and Fig. 11. It can be seen from Fig. 10 and Fig. 11 that the proposed protection can trip correctly within 30ms after the occurrence of grounding faults, and has strong tolerance to fault resistance.

TABLE I
OPERATION PERFORMANCE AFTER CHANGE OF OPERATION MODE OF POWER GRID

Fault resistance(Ω)	Fault type	Fault location	t^{I}(ms)	t^{II}(ms)	$\alpha(t=150ms)$
1	AB	50%	38	37	0.498
		75%	39	38	0.751
	ABG	50%	27	26	0.500
		75%	28	27	0.750
	AG	50%	25	25	0.500
		75%	25	25	0.747
10	AB	50%	39	39	0.499
		75%	40	40	0.755
	ABG	50%	26	25	0.506
		75%	27	26	0.751
	AG	50%	24	23	0.504
		75%	24	23	0.749
100	AB	50%	39	38	0.502
		75%	39	38	0.748
	ABG	50%	25	25	0.548
		75%	22	21	0.762
	AG	50%	24	23	0.535
		75%	25	25	0.750

TABLE II
OPERATION PERFORMANCE OF PROPOSED PROTECTION WHEN PF ≠ 1

Fault resistance(Ω)	Fault type	Fault location	t^{I}(ms)	t^{II}(ms)	$\alpha(t=150ms)$
1	AB	50%	37	36	0.499
		75%	40	36	0.748
	ABG	50%	23	24	0.510
		75%	28	24	0.752
	AG	50%	25	23	0.501
		75%	25	23	0.747
10	AB	50%	29	27	0.498
		75%	29	27	0.754
	ABG	50%	27	25	0.504
		75%	27	26	0.745
	AG	50%	24	23	0.501
		75%	25	24	0.755
100	AB	50%	35	34	0.497
		75%	31	29	0.745
	ABG	50%	25	23	0.524
		75%	28	26	0.763
	AG	50%	27	24	0.514
		75%	27	25	0.759

D. Different Operation Modes of Power Grid

By adjusting the internal impedance of the power source, the change of the operation mode of power grid is simulated. Table I shows the operation performance of proposed protection after the change of operation mode of power grid when asymmetric faults occur at 50% and 75% of L87 with different fault resistance. It can be seen from Table I that the proposed protection can trip correctly. Since the equivalent impedance of power grid is calculated in real-time by local measurements, the proposed protection is adaptive to the change of operation mode of power grid.

E. GCs of Different Regions

In the previous parts, the simulation with no reactive power support (PF=1) is studied, and the simulation with reactive power support (PF≠1) is carried out in this part.

Reactive power support is provided for power grid according to German GC [16]. When asymmetric faults occur at 50% and 75% of L87 with different fault resistance, the operation performance of proposed protection is shown in Table II. Different reactive power support strategies do not change the analytical model of additional impedance (5), so the proposed protection can still calculate the fault location and trip correctly. To sum up, the proposed protection can operate normally under different reactive power support strategies. Therefore, the proposed protection can adapt to GCs of different regions.

TABLE III
OPERATION PERFORMANCE OF PROPOSED PROTECTION UNDER DIFFERENT CAPACITY OF IIRPP WITH 100 Ω FAULT RESISTANCE

P_{IIRPP} [a] (MW)	Fault type	Fault location	t^{I}(ms)	t^{II}(ms)	$\alpha(t=150ms)$
50	AB	50%	40	40	0.502
		75%	31	30	0.752
	ABG	50%	29	29	0.525
		75%	29	29	0.761
	AG	50%	27	27	0.518
		75%	27	27	0.767
25	AB	50%	40	40	0.512
		75%	31	30	0.758
	ABG	50%	29	29	0.547
		75%	29	29	0.769
	AG	50%	27	27	0.538
		75%	27	27	0.762

[a] P_{IIRPP} is the capacity of IIRPP.

F. Different Capacity of IIRPP

When the capacity of IIRPP is set as 50MW and 25MW, and asymmetric faults occur at 50% and 75% of L87 with 100Ωfault resistance, operation performance of proposed protection is shown in Table III.

The capacity of IIRPP do not change the analytical model of additional impedance (5), so the change of IIRPP capacity has little effect on α calculated by proposed protection. In conclusion, the proposed protection is not affected by the capacity of IIRPP.

G. Operation Performance Comparison of Proposed Protection with Existing Protections

Table IV shows the operation performance comparison of proposed protection with existing protections. In Table IV, "–" means that the protection scheme does not occupy the control system. Subscripts d and q represent the d-axis and q-axis components in the synchronous reference frame.

It can be seen from Table IV that compared with [13], the proposed protection in this paper requires no communication. In addition, the trip time of protection scheme proposed in this paper is faster than that of proposed protection in [14]. Compared with [16] and [17], the proposed protection in this paper does not occupy the control system, so it can adapt to different reactive power support strategies.

VI. CONCLUSIONS

Due to the weak infeed and controlled current phase of IIRPP, traditional distance protection on IIRPP-side of the outgoing line of IIRPP is in danger of overreach or underreach during asymmetric faults. This paper analyzes the composite sequence

TABLE IV
OPERATION PERFORMANCE COMPARISON OF PROPOSED PROTECTION WITH EXISTING PROTECTIONS

Method	Trip time during PP faults	Trip time during PPG and SPG faults	Communication	Adjusted control parameters
Reference [13]	Within two cycles	Within two cycles	Requirement	–
Reference [14]	About 300ms	About 70ms	No requirement	–
Reference [16]	Within two cycles	Within two cycles	No requirement	$i_d^{(+)}$, $i_q^{(+)}$
Reference [17]	Within two cycles	Within two cycles	No requirement	$i_d^{(+)}$, $i_q^{(+)}$, $i_d^{(-)}$, $i_q^{(-)}$
Proposed protection	Within two cycles	Within two cycles	No requirement	–

network of the outgoing line of IIRPP during asymmetric faults, and proposes an adaptive distance protection based on the analytical model of additional impedance.

The proposed protection has the following advantages:

1) Based on the open circuit property of IIRPP-side in negative-sequence network, the equivalent impedance of power grid and the current at fault point can be obtained in real-time by local measurements, so the proposed protection has strong tolerance to fault resistance in the system with weak sources.

2) The equivalent impedance of power grid is calculated by local measurements, and the proposed protection is adaptive to the change of operation mode of power grid.

3) The analytical model of additional impedance proposed in this paper is immune to various reactive power support strategies and the capacity of IIRPP, so the proposed protection can adapt to different requirements of GCs for reactive power support and different capacity of IIRPP.

APPENDIX A

Take the arctangent function on both sides of equation (9) and note that the left-side is $f(\alpha)$ and the right-side is $h(\alpha)$. The following equation can be obtained.

$$\begin{aligned}&\underbrace{\arctan\left[\frac{|Z_m|\sin\varphi_m-\alpha\cdot|Z_L|\sin\varphi_L}{|Z_m|\cos\varphi_m-\alpha\cdot|Z_L|\cos\varphi_L}\right]}_{f(\alpha)}\\&=\underbrace{\angle\frac{U_{CL}^{(-)}}{I_{CL}^{(+)}}-\arctan\left[\frac{|Z_S|\sin\varphi_S+(1-\alpha)|Z_L|\sin\varphi_L}{|Z_S|\cos\varphi_S+(1-\alpha)|Z_L|\cos\varphi_L}\right]}_{h(\alpha)}\end{aligned}\tag{21}$$

The following equation can be obtained by deriving α from both sides of (21):

$$\begin{cases}d[f(\alpha)]/d\alpha=|Z_L|\cdot|Z_m|\sin(\varphi_m-\varphi_L)/\left(E_1^{\,2}+E_2^{\,2}\right)\\d[h(\alpha)]/d\alpha=|Z_L|\cdot|Z_S|\sin(\varphi_L-\varphi_S)/\left(E_3^{\,2}+E_4^{\,2}\right)\end{cases}\tag{22}$$

where E_1, E_2, E_3 and E_4 are as follows.

$$\begin{cases}E_1=\alpha|Z_L|\cos\varphi_L-|Z_m|\cos\varphi_m\\E_2=\alpha|Z_L|\sin\varphi_L-|Z_m|\sin\varphi_m\\E_3=|Z_S|\sin\varphi_S+(1-\alpha)|Z_L|\sin\varphi_L\\E_4=|Z_S|\cos\varphi_S+(1-\alpha)|Z_L|\cos\varphi_L\end{cases}\tag{23}$$

It can be seen from (22) that the monotonicity of $f(\alpha)$ is determined by φ_m and φ_L, and the monotonicity of $h(\alpha)$ is determined by φ_L and φ_S.

1) *Case1: the monotonicity of $f(\alpha)$ and $h(\alpha)$ is opposite*

This case includes two combinations: $f(\alpha)$ increases monotonically, and $h(\alpha)$ decreases monotonically; $f(\alpha)$ decreases monotonically, and $h(\alpha)$ increases monotonically. The schematic diagram of $f(\alpha)$ and $h(\alpha)$ is shown in Fig. 12.

$f(\alpha)$ and $h(\alpha)$ have only one intersection point on $[-\infty, +\infty]$ (see Appendix B for detailed proof), and the abscissa of this intersection point is the actual fault location, which is recorded as α_{true}. Since the period of the tangent function is π, (21) can also be written as follows:

$$\begin{aligned}&\arctan\left[\frac{|Z_m|\sin(\varphi_m)-\alpha\cdot|Z_L|\sin(\varphi_L)}{|Z_m|\cos(\varphi_m)-\alpha\cdot|Z_L|\cos(\varphi_L)}\right]+k\pi\\&=\angle\frac{U_{CL}^{(-)}}{\left[Z_S+(1-\alpha)\cdot Z_L\right]\cdot I_{CL}^{(+)}}\Rightarrow f(\alpha)+k\pi=h(\alpha)\end{aligned}\tag{24}$$

where k=0, ±1, ±2…. The relationship between $f(\alpha)+k\pi$ and $h(\alpha)$ is as shown in Fig. 12. It can be seen from Fig. 12 that $f(\alpha)\pm\pi$ and $h(\alpha)$ have another intersection point. The abscissa of this intersection point is the invalid solution, which is recorded as α_{false}. The characteristics of α_{false} are described below.

According to the physical meaning of $f(\alpha)$, $X(\alpha)$ and $\sin(f(\alpha))$ have the same sign. Therefore, α_{true} in Fig. 12 has the property that $X(\alpha_{true})$ and $\sin(f(\alpha_{true}))$ have the same sign. On the contrary, because the sine function has the property that $\sin(\varphi\pm\pi)=-\sin(\varphi)$, α_{false} in Fig. 12 has the property that $X(\alpha_{false})$ and $\sin(f(\alpha_{false})\pm\pi)$ have the opposite sign. According to this property, an equality constraint is added, as shown in the following equation.

$$X(\alpha)/\left|X(\alpha)\right|=\sin h(\alpha)/\left|\sin h(\alpha)\right|\tag{25}$$

2) *Case2: the monotonicity of $f(\alpha)$ and $h(\alpha)$ is the same*

This case includes two combinations: $f(\alpha)$ and $h(\alpha)$ decrease monotonically; $f(\alpha)$ and $h(\alpha)$ increase monotonically. The schematic diagram of $f(\alpha)$ and $h(\alpha)$ is shown in Fig. 12. In this case, $f(\alpha)$ and $h(\alpha)$ have one solution respectively in $[-\infty, 0]$ and $[0, +\infty]$ (see Appendix C for detailed proof).

According to the protection scheme in this paper, the protection returns during reverse faults, so the faults calculated by (10) are forward faults. Therefore, α should be greater than 0, and the solution less than 0 is invalid. According to this property, an inequality constraint is added, as shown in the following inequality.

$$\alpha>0\tag{26}$$

In conclusion, the invalid solutions can be eliminated according to (25) and (26).

APPENDIX B

Taking $f(\alpha)$ monotonically decreasing and $h(\alpha)$ monotonically increasing as an example. The following equation can be obtained from Fig. 5.

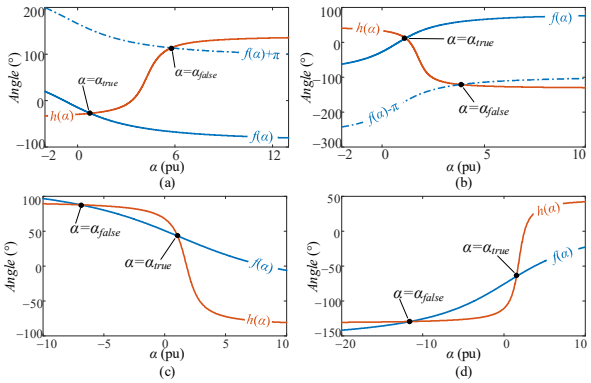

Fig. 12 Schematic diagram of $f(\alpha)$ and $h(\alpha)$. (a) $f(\alpha)$ decreases monotonically, and $h(\alpha)$ increases monotonically. (b) $f(\alpha)$ increases monotonically, and $h(\alpha)$ decreases monotonically. (c) $f(\alpha)$ and $h(\alpha)$ decrease monotonically. (d) $f(\alpha)$ and $h(\alpha)$ increase monotonically.

$$\angle\frac{U_{CL}^{(-)}}{I_{CL}^{(+)}}=\angle\left[\left(\frac{U_{CL}^{(+)}}{I_{CL}^{(+)}}-\alpha Z_L\right)\frac{Z_S+(1-\alpha)Z_L}{Z_S+(1-\alpha)Z_L+R}\right] \tag{27}$$

During faults, the IIRPP will inject active or reactive power, so the range of $\angle[U_{CL}^{(+)}/I_{CL}^{(+)}]$ is $[-\pi/2, 0]$. According to (27), the range of $\angle[U_{CL}^{(-)}/I_{CL}^{(+)}]$ is $[\varphi_L-\pi, \pi/2]$. Therefore, the relations of $f(-\infty)$, $h(-\infty)$, $f(+\infty)$, and $h(+\infty)$ are as follows.

$$\begin{cases} h(-\infty)=\angle U_{CL}^{(-)}/I_{CL}^{(+)}-\varphi_L\le\dfrac{\pi}{2}-\varphi_L<\varphi_L=f(-\infty) \\ h(+\infty)=\angle U_{CL}^{(-)}/I_{CL}^{(+)}-\varphi_L+\pi\ge 0>\varphi_L-\pi=f(+\infty) \end{cases} \tag{28}$$

According to the zero-point theorem, $f(\alpha)$ and $h(\alpha)$ have only one solution in $[-\infty, +\infty]$. The same conclusion is obtained when $f(\alpha)$ increases and $h(\alpha)$ decreases monotonically.

APPENDIX C

Taking $f(\alpha)$ and $h(\alpha)$ monotonically decreasing as an example (In this example, $\varphi_m<\varphi_L$ and $\varphi_L<\varphi_S$).

When a fault occurs, Z_m can be expressed as follows.

$$Z_m=\alpha Z_L+R_{ph}\frac{U_{CL}^{(-)}}{\left[Z_S+(1-\alpha_{real})Z_L\right]\cdot I_{CL}^{(+)}} \tag{29}$$

Due to the weak infeed of IIRPP, the amplitude of Z_{add} is much larger than the mode of αZ_L, and the phase of Z_m is almost equal to the phase of Z_{add}. Therefore, the derivation is as follows.

$$f(0)\approx\angle\frac{U_{CL}^{(-)}}{\left[Z_S+(1-\alpha_{real})Z_L\right]\cdot I_{CL}^{(+)}}=h(\alpha_{real})<h(0) \tag{30}$$

According to Appendix B, the range of $\angle[U_{CL}^{(-)}/I_{CL}^{(+)}]$ is $[\varphi_L-\pi, \pi/2]$, from which it can be concluded that $f(-\infty)>h(-\infty)$ and $f(+\infty)>h(+\infty)$. According to the zero-point theorem, it can be concluded that $f(\alpha)$ and $h(\alpha)$ have two intersections, which are located at $[-\infty, 0]$ and $[0, +\infty]$. When $f(\alpha)$ and $h(\alpha)$ are monotonically increasing, the same conclusion is obtained.

REFERENCES

[1] F. Blaabjerg, R. Teodorescu, M. Liserre and A. V. Timbus, "Overview of control and grid synchronization for distributed power generation systems," IEEE Trans. Ind. Electron., vol. 53, no. 5, pp. 1398-1409, Oct. 2006.

[2] A. Hooshyar, M. A. Azzouz and E. F. El-Saadany, "Distance Protection of Lines Emanating From Full-Scale Converter-Interfaced Renewable Energy Power Plants—Part I: Problem Statement," IEEE Trans. Power Deliv., vol. 30, no. 4, pp. 1770-1780, Aug. 2015.

[3] IEEE Guide for Protective Relay Applications to Transmission Lines, IEEE Std C37.113-2015, 2016.

[4] Y. Q. Xia, K. K. Li and A. K. David, "Adaptive relay setting for stand-alone digital distance protection," in IEEE Trans. Power Deliv., vol. 9, no. 1, pp. 480-491, Jan. 1994.

[5] P. Mishra, A. K. Pradhan and P. Bajpai, "Adaptive Distance Relaying for Distribution Lines Connecting Inverter-Interfaced Solar PV Plant," IEEE Trans. Ind. Electron., vol. 68, no. 3, pp. 2300-2309, March 2021.

[6] J. Ma, W. Ma, Y. Qiu and J. S. Thorp, "An Adaptive Distance Protection Scheme Based on the Voltage Drop Equation," IEEE Trans. Power Deliv., vol. 30, no. 4, pp. 1931-1940, Aug. 2015.

[7] Y. Liang, Z. Lu, W. Li, W. Zha and Y. Huo, "A Novel Fault Impedance Calculation Method for Distance Protection Against Fault Resistance," IEEE Trans. Power Deliv., vol. 35, no. 1, pp. 396-407, Feb. 2020.

[8] V. H. Makwana and B. R. Bhalja, "A New Digital Distance Relaying Scheme for Compensation of High-Resistance Faults on Transmission Line," IEEE Trans. Power Deliv., vol. 27, no. 4, pp. 2133-2140, Oct. 2012.

[9] J. Ma, C. Liu, Y. Zhao, S. Kang and J. S. Thorp, "An Adaptive Overload Identification Method Based on Complex Phasor Plane," IEEE Trans. Power Deliv., vol. 31, no. 5, pp. 2250-2259, Oct. 2016.

[10] Y. Liang, W. Li, Z. Lu, G. Xu and C. Wang, "A New Distance Protection Scheme Based on Improved Virtual Measured Voltage," IEEE Trans. Power Deliv., vol. 35, no. 2, pp. 774-786, April 2020.

[11] K. Xu, Z. Zhang, Q. Lai and X. Yin, "Fault phase selection method applied to tie line of renewable energy power stations," IET Gener. Transm. Distrib., vol. 14, no. 13, pp. 2549-2557, May. 2020.

[12] K. Jia, Z. Yang, Y. Fang, T. Bi and M. Sumner, "Influence of Inverter-Interfaced Renewable Energy Generators on Directional Relay and an Improved Scheme," IEEE Trans. Power Electron., vol. 34, no. 12, pp. 11843-11855, Dec. 2019.

[13] A. Hooshyar, M. A. Azzouz and E. F. El-Saadany, "Distance Protection of Lines Emanating From Full-Scale Converter-Interfaced Renewable Energy Power Plants—Part II: Solution Description and Evaluation," IEEE Trans. Power Deliv., vol. 30, no. 4, pp. 1781-1791, Aug. 2015.

[14] Y. Fang, K. Jia, Z. Yang, Y. Li and T. Bi, "Impact of Inverter-Interfaced Renewable Energy Generators on Distance Protection and an Improved Scheme," IEEE Trans. Ind. Electron., vol. 66, no. 9, pp. 7078-7088, Sept. 2019.

[15] K. Jia, C. Gu, Z. Xuan, L. Li and Y. Lin, "Fault Characteristics Analysis and Line Protection Design Within a Large-Scale Photovoltaic Power Plant," IEEE Trans. Smart Grid, vol. 9, no. 5, pp. 4099-4108, Sept. 2018.

[16] A. Banaiemoqadam, A. Hooshyar and M. A. Azzouz, "A Control-Based Solution for Distance Protection of Lines Connected to Converter-Interfaced Sources During Asymmetrical Faults," IEEE Trans. Power Deliv., vol. 35, no. 3, pp. 1455-1466, June 2020.

[17] A. Banaiemoqadam, A. Hooshyar and M. A. Azzouz, "A Comprehensive Dual Current Control Scheme for Inverter-Based Resources to Enable Correct Operation of Protective Relays," IEEE Trans. Power Deliv., doi: 10.1109/TPWRD.2020.3025878.

[18] Hong-Seok Song and Kwanghee Nam, "Dual current control scheme for PWM converter under unbalanced input voltage conditions," IEEE Trans. Ind. Electron., vol. 46, no. 5, pp. 953-959, Oct. 1999.

[19] J. Jia, G. Yang and A. H. Nielsen, "A Review on Grid-Connected Converter Control for Short-Circuit Power Provision Under Grid Unbalanced Faults," IEEE Trans. Power Deliv., vol. 33, no. 2, pp. 649-661, April 2018.

[20] Z. Xu, S. Jiang, Q. Yang and T. Bi, "Ground distance relaying algorithm for high-resistance fault," IET Gener. Transm. Distrib., vol. 14, no. 13, pp. 2549-2557, May. 2020.

[21] A. Hooshyar, E. F. El-Saadany and M. Sanaye-Pasand, "Fault Type Classification in Microgrids Including Photovoltaic DGs," IEEE Trans. Smart Grid, vol. 7, no. 5, pp. 2218-2229, Sept. 2016.

[22] M. S. El Moursi, W. Xiao, and J. L. Kirtley, "Fault ride through capability for grid interfacing large scale PV power plants," IET Gener. Transm. Distrib., vol. 7, no. 9, pp. 1027–1036, Sep. 2013.

[23] Technical Requirements for Connecting Photovoltaic Power Station to Power System, GB/T 19964-2012, 2013(In Chinese).